

Distributed Bragg grating integrated-optical filters: Synthesis and fabrication

V. V. Wong,^{a)} J. Ferrera, J. N. Damask, T. E. Murphy, Henry I. Smith, and H. A. Haus
*Department of Electrical Engineering and Computer Science, Massachusetts Institute of Technology,
Cambridge, Massachusetts 02139*

(Received 19 June 1995; accepted 9 August 1995)

The design, fabrication, and measurement of planar, passive Bragg grating-based transmission filters is presented. We combine interferometric lithography, spatial-phase-locked electron-beam lithography, x-ray nanolithography, and optical lithography with silica-on-silicon waveguiding substrates to define rib waveguides and grating patterns that have multiple quarter-wave shifts along the grating length. Transmission filters such as Gaussian, Butterworth, and Chebyshev can be designed and fabricated with these technologies. © 1995 American Vacuum Society.

I. CONSTRUCTION OF BRAGG GRATING FILTERS

In order to increase the aggregate bit rate of wavelength-division multiplexed optical communication systems, channel density can be increased by reducing the interchannel spacing. As the channel spacing is reduced, however, the bandwidth of the optical filters that are used to separate the channels must be commensurately reduced. One way to implement a narrow-band filter is to use a quarter-wave shifted Bragg grating resonator.¹⁻³ This resonant filter, called a single-pole filter (SPF), is inherently limited to a rolloff of -10 dB/decade away from resonance, regardless of the bandwidth. In order to increase the filter rolloff, thereby decreasing the crosstalk between channels while retaining the filter bandwidth, several resonators can be coupled to produce a so-called multiple-pole filter (MPF).

To realize single- and multiple-pole passive, planar Bragg grating-based filters, we have used a strip-loaded rib waveguide geometry where a grating pattern is etched onto the rib stripe. The period of the grating is fixed at the Bragg period, or $\Lambda = \lambda_0/2n_{\text{eff}}$, where λ_0 is the free-space wavelength, and n_{eff} is the effective index of the waveguide. A uniform grating at the Bragg period reflects those frequencies that lie within the so-called stopband back along the waveguide. The strength of the grating, denoted by κ , is a measure of the reflection strength of each grating tooth. To generate the optical resonances, one or more quarter-wave shifts are inserted at appropriate locations along the length of the grating. By designing the correct grating pattern, the optical resonances can be manipulated to produce the desired filter spectral response. The problem of filter synthesis therefore rests on the design of grating patterns. Yet, it is important to appreciate that the intimate connection between the grating pattern and the spectral response of this class of passive optical filters requires that the grating pattern faithfully reproduce the mathematically determined pattern. There must be no chirp or abrupt gaps or overlaps along the length of the as-written grating because such deviations translate into deterioration of the spectral response. In other words, the as-written grating patterns must be as coherent as the light with which they are to interact.

Our approach to fabricate passive grating-based filters is

to combine interferometric lithography, spatial-phase-locked electron-beam lithography (SPLEBL),⁴ x-ray nanolithography (XRNL),⁵ and optical lithography with silica-on-silicon waveguiding substrates. Optical lithography is used to define the waveguide rib stripes. Spatial-phase-locked electron-beam lithography is combined with interferometrically defined fiducial references to write highly coherent grating patterns that can span over 2 mm in length. The grating patterns are written onto an x-ray mask which in turn is used to transfer the grating patterns to the top of the rib waveguides. Reactive ion etching is used to etch both the rib and grating patterns. The grating patterns themselves are designed using waveguide optical parameters and standard filter synthesis techniques. We have designed, fabricated, and tested filters with one and more quarter-wave shifts inserted along the length of the grating. This article outlines the entire filter-making process from design to measurement, and details some of the problems that we have encountered.

A. Single-pole filters

In 1976 Haus and Shank¹ showed that the insertion of a quarter-wave shift at the center of an otherwise coherent Bragg grating supports a single high- Q resonance at the Bragg wavelength, Fig. 1(a). At resonance, optical energy is stored in the resonator and the field amplitude decays exponentially to either side of the quarter-wave shift at $z=0$ as $\exp[-\kappa|z|]$. Energy escapes from the resonator at the grating ends because the field there does not decay to zero. The inverse Q parameter, defined as the power that escapes from the resonator per cycle divided by the stored energy, is given as

$$\frac{1}{Q} = \frac{2\kappa\lambda_0}{\pi n_g} e^{-2\kappa n \Lambda}, \quad (1)$$

where n_g is the group index of the mode, n is the number of teeth in each grating arm, and $n\Lambda$ is the length of the arm. The Q parameter also relates the resonance linewidth $\Delta\nu$ to the center frequency ν_0 , as $1/Q = \Delta\nu/\nu_0$. Equating this definition with Eq. (1), and after rearrangement, the number of teeth in each grating arm can be expressed in waveguide parameters and the desired filter response alone:

$$n = \frac{1}{2\kappa\Lambda} \ln \left[\frac{2\kappa c}{\pi n_g \Delta\nu} \right], \quad (2)$$

^{a)}Current address: SDL, Inc., 80 Rose Orchard Way, San Jose, CA 95134-1365.

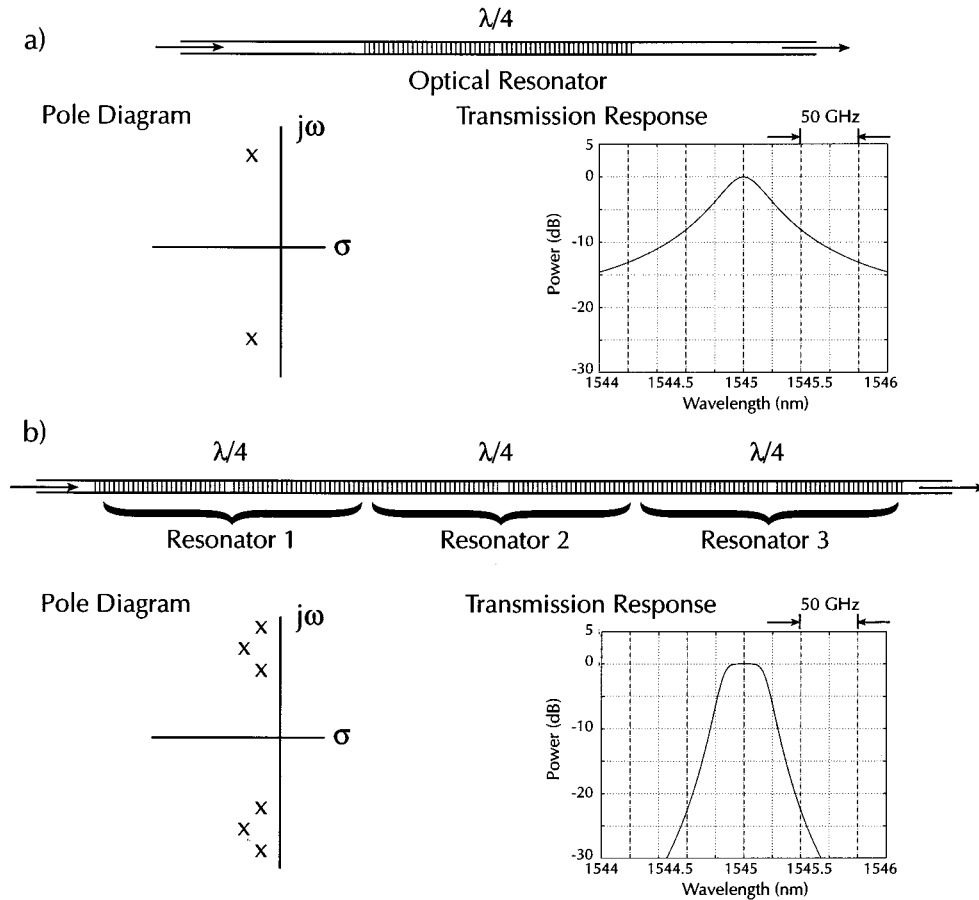


FIG. 1. (a) A Bragg grating with a single quarter-wave shift at the center can be modeled as a single-pole filter near resonance. The pole diagram shows one complex conjugate pole pair. The transmission response shows the filter spectrum near resonance, with 50 GHz spaced lines indicating the channel locations of a WDM system. (b) Three coupled single-pole resonators create a multiple-pole filter, as indicated on the pole diagram. With proper grating design, the near-resonance spectrum can look like that shown in the transmission response.

where c is the speed of light. While Eq. (2) can be used to generate a grating pattern for nearly any full width at half-maximum (FWHM) resonance, consideration of the entire spectral response is necessary to determine the discrimination level between transmitted and reflected wavelengths.

B. Multiple-pole filters

Haus et al. showed in 1977² and again in 1992³ that multiple-pole filter (MPF) responses such as Butterworth, Chebyshev, and Gaussian, can be synthesized by cascading several single-pole filters of the same frequency, Fig. 1(b). The resonators couple to one another across the grating lengths, thereby splitting the frequency degeneracy. Together with the correct formalism, standard filter synthesis tables can be used to design the grating patterns.

Consider the cascade of three resonators shown in Fig. 2(a). Each resonator has an arm length l_i , and a Q parameter Q_i . Equation (1) relates Q_i to l_i through the optical and filter parameters. Moreover, the Q parameters of each resonator can be related to a reference Q value via

$$\frac{1}{Q_r} = \frac{2\kappa\lambda_0 Q_i / Q_r}{\pi n_g} e^{-2\kappa l_i}, \tag{3}$$

where $1/Q_r = \Delta\nu_r/\nu_0$. Rearranging Eq. (3) and replacing l_i with $n_i\Lambda$, the number of teeth in each arm of the i th resonator, yields

$$n_i = \frac{1}{2\kappa\Lambda} \ln \left[\frac{2\kappa c C_i}{\pi n_g \Delta\nu_r} \right], \tag{4}$$

where $\Delta\nu_r$ is the nominal single-pole FWHM bandwidth and $C_i = Q_i/Q_r$. While n_i is the number of teeth in each arm of the i th resonator, the number of teeth between adjacent quarter-wave shifts is $N_i = n_i + n_{i-1}$, see Fig. 2(a).

Table I lists the Q scaling values for odd-order Butterworth filters up to ninth order.⁶ The table also lists the associated grating patterns for each filter, given the parameters $\kappa = 120 \text{ cm}^{-1}$, $n_g = 1.72$, $\Lambda = 521 \text{ nm}$, and $\Delta\nu_r = 75 \text{ GHz}$ (suitable for testing purposes). A quarter-wave shift is placed after every N_i teeth.

C. Grating pattern layout

The grating patterns for Butterworth filters, as presented in Table I, are composed of hundreds or thousands of grating teeth that can span over 2 mm in length. Other classes of MPFs have similar dimensions. In order to write this pattern with electron-beam lithography (EBL), the pattern must be

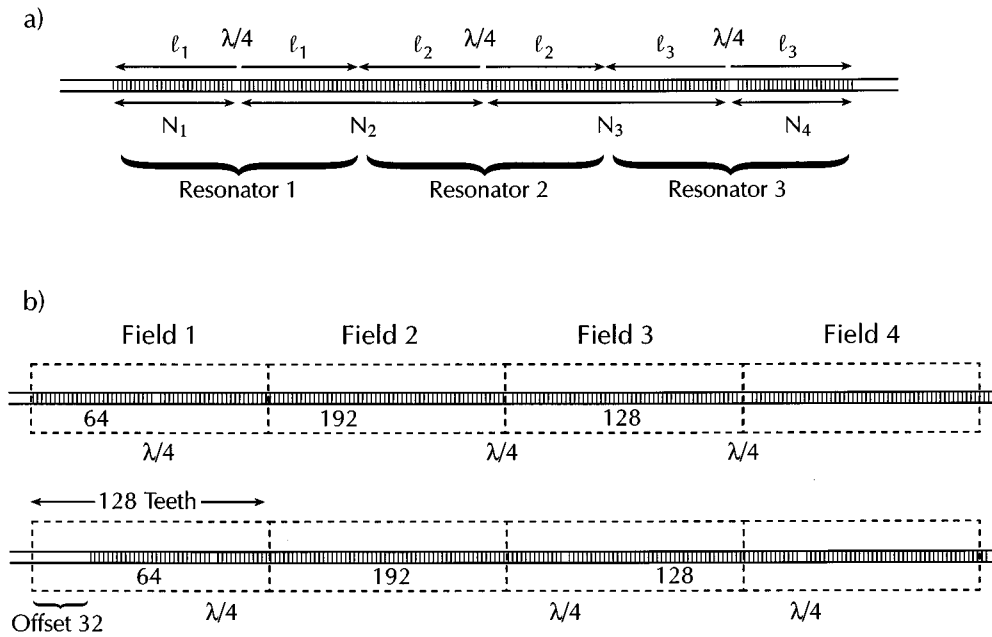


FIG. 2. (a) Three coupled single-pole resonators. Equation (4) gives the lengths $ℓ_i = n_iΛ$, as indicated in the figure. The number of teeth between adjacent quarter-wave shifts is given by $N_i = n_i + n_{i-1}$. (b) Two ways to lay out a grating with a pattern of $N = 64, 192, 128, …$. The upper case inserts no blank offset teeth in the left-most field, resulting in the latter two quarter-wave shifts being placed on a field boundary. The second case inserts 32 blank teeth in the left-most field, with the result that all quarter-wave shifts are 32 teeth away from the closest field boundary.

fractured into grating segments one EBL-field long, and each grating segment written in turn. Stitching errors at field boundaries correspond to phase errors along the grating which in turn distort the filter’s spectral response. The degree of distortion depends on the magnitude of the phase error and its location with respect to a quarter-wave shift. A phase error located halfway in between two quarter-wave shifts has less effect than the same phase error located at one of the quarter-wave shifts.

In order to place the quarter-wave shifts as far from a field boundary as possible, an offset of blank teeth can be added to the first field of the pattern. Consider the example in Fig. 2(b) where the hypothetical grating pattern is $N = 64, 192, 128, …$ and the number of teeth in each field is 128. In case (a), no offset is added with the result that the second and third quarter-wave shifts lie on a field boundary.

In Fig. 2(b), however, an offset of 32 blank teeth in the first field leads to all three quarter-wave shifts 32 teeth away from any field boundary. To fracture the actual grating patterns, a computer program was written to repeatedly fracture a pattern with offsets that ranged from 0 to 127. The offset that left all quarter-wave shifts as far from any field boundary as possible was chosen.

II. FABRICATION

The waveguide substrate was made by three successive film depositions onto high-resistivity 10-cm diam silicon wafers: 4.0- $μ\text{m}$ -thick wet SiO_2 diffusion for the lower cladding; 154-nm-thick low-pressure chemical vapor deposition (LPCVD) Si_3N_4 , subsequently annealed for 2 h at 1000 °C; and 340 nm LPCVD low-temperature SiO_2 , subsequently

TABLE I. Q scaling values for odd order Butterworth filters up to ninth order.^a

Order	C_1	C_2	C_3	C_4	C_5	C_6	C_7	C_8	C_9
1	2.0000								
3	1.0000	2.0000	1.0000						
5	0.6180	1.6180	2.0000	1.6180	0.6180				
7	0.4450	1.2470	1.8019	2.0000	1.8019	1.2470	0.4450		
9	0.3473	1.0000	1.5321	1.8794	2.0000	1.8794	1.5321	1.0000	0.3473

Order	N_1	N_2	N_3	N_4	N_5	N_6	N_7	N_8	N_9	N_{10}
1	286	286								
3	230	516	516	230						
5	192	461	555	555	461	192				
7	165	413	525	563	563	525	413	165		
9	146	376	494	545	567	567	545	494	376	146

^a $\kappa = 120 \text{ cm}^{-1}$, $n_g = 1.72$, $\Delta\nu_r = 75 \text{ GHz}$, $\Lambda = 521 \text{ nm}$.

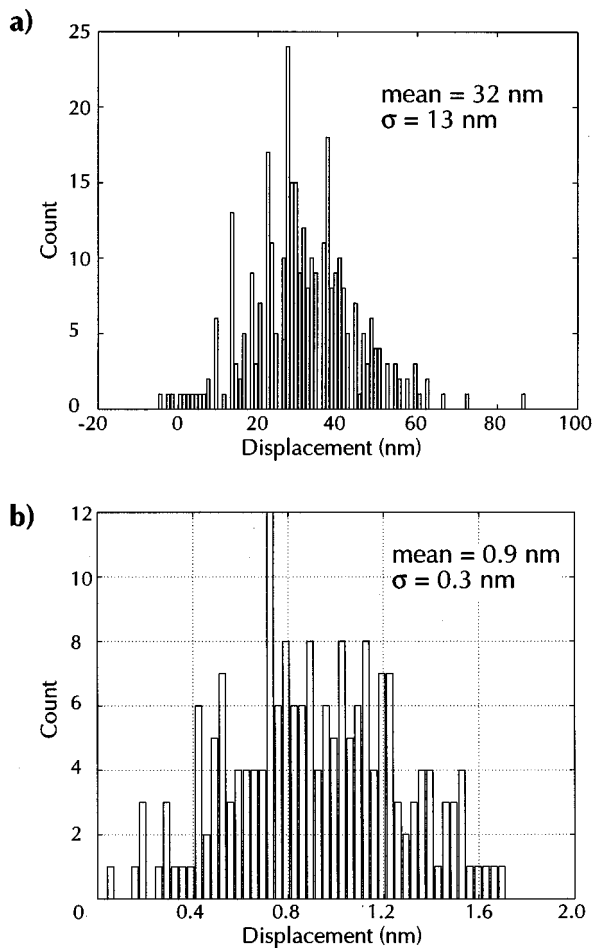


FIG. 3. (a) Distribution of interfield stitching errors on single-pole filter mask as measured with outrigger patterns and Fourier techniques. (b) Distribution of a representative subset of interfield stitching errors on some mask as measured between the e-beam field border and the fiducial reference grating prior to writing the grating segments.

annealed for 2 h at 950 °C, which reduced the thickness to 315 nm. Rib waveguides were then patterned using optical projection lithography and etched to a target depth of 200 nm via reactive ion etching.

The essential steps of the remainder of the fabrication process were described previously.⁵ The self-aligned process was used in all cases, and the environmentally stable chemically amplified positive ESCAP resist,⁷ was spun on as the imaging layer for the Bragg gratings. The high sensitivity and stability of the ESCAP allowed a step-and-repeat procedure to be implemented as follows.

After the lift off of the chromium, an adhesion promoter, hexamethyl disilazane (HMDS), was spun on, followed by 400 nm of ESCAP, which was baked on a vacuum hotplate at 150 °C for 90 s. Following this, an alignment was performed between the x-ray mask containing the Bragg gratings and the substrate containing the optical waveguides. Once aligned, an x-ray exposure of one 6×4 mm die was performed using the Cu_L line ($\lambda = 1.32$ nm). After exposure, two additional mask-to-substrate alignments and x-ray exposures were performed, after which the ESCAP was postbaked on a vacuum hotplate at 142 °C for 40 s.

All three of the exposed dice were then developed simultaneously in Microposit MF321. Although the first die which was exposed experienced an 8 h delay between x-ray exposure and postexposure bake, the resist profiles of this die were comparable to those of the other two dies. After development, the Bragg gratings were transferred into the top SiO₂ cladding layer by reactive ion etching in CHF₃. At this point the ESCAP was stripped in an oxygen plasma and the substrate cleaned in a solution of H₂O:H₂O₂:NH₄OH at 80 °C for 10 min. Once again, HMDS was spun-on followed by a 400-nm-thick layer of ESCAP, and another series of three alignment and exposures performed. By repeating this process, nine separate dice (three sets of 3) were successfully step-and-repeated on the substrate. After the pattern transfer of the last set of dice, the ESCAP was stripped in an oxygen plasma and the chromium was stripped. The multiplicity of dice on one substrate allows one to etch each die set to a different depth. In this way, the grating strength can be varied across a single wafer which allows for a more accurate analysis of the effects of the grating strength on device performance.

A. Etching

The grating patterns for a particular filter are designed for a predetermined grating strength. If there is an error during fabrication which leads to a grating strength that is larger than the design value, the resonators will be undercoupled, which in turn narrows the filter response and decreases the rate of rolloff away from the filter center. A grating strength that is less than the design value overcouples the resonators, which results in a filter that is too wide and with greater ripple in the passband. Since the grating strength is related to the waveguide layer indices, thicknesses, and rib and grating etch depths, all waveguide dimensions must be accurately controlled. Ellipsometry was used to determine the thickness of the waveguide layers after each film deposition.

In order to achieve a high degree of control for the grating etch depth, a two-step dry-etching procedure was developed. Based on the etch rate of monitor samples, the first etch step was calculated to achieve a depth close to but less than the target depth. After the etch, a thin quartz disk with a square hole the size of one chip is placed on the wafer so as to expose the die for plasma removal of the ESCAP resist. The depth of the etch is then measured. Based on the difference between the measured and target depths, a second etch time is calculated and the remaining dice are etched accordingly. When compared to a single-etch procedure, the uncertainty in final etch depth by this method is reduced by a factor of approximately the ratio of the second to the total etch durations. After using the two-step etch procedure to achieve an etch depth of 150 nm, etch depths of 151 ± 2 and 150 ± 2 nm were measured by ellipsometry and profilometry, respectively.

III. INTERFIELD ERROR RESULTS

In order to measure the stitching errors between adjacent grating segments, “outrigger” structures were written at each segment boundary.⁴ Each outrigger pattern consists of two gratings written in two separate e-beam fields, but located side by side so that the grating lines nominally line up. Each

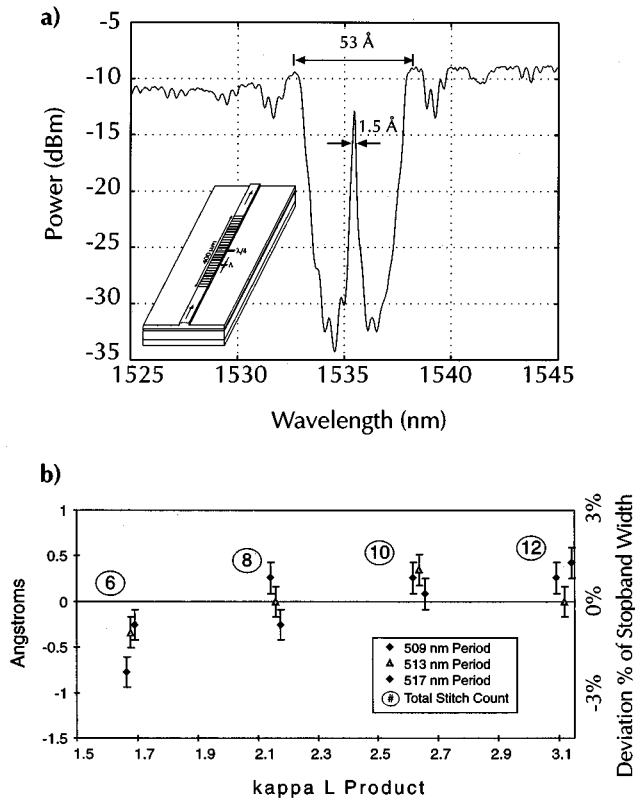


Fig. 4. (a) The optical transmission response of single-pole filter written across nine e-beam fields. The stopband width is 53 Å and the resonance FWHM linewidth is approximately 1.5 Å. (b) The measured deviation from the stopband center of resonances from 12 resonators of different lengths and periods. The encircled numbers are the number of field stitchings.

grating has the same spatial period as the resonator grating, is 8 periods long and 2 μm wide, and is oriented so that the grating lines are perpendicular to the waveguide axis. Two outrigger structures were written at each segment boundary, approximately 20 μm above and below the device grating. With this configuration, the stitching error between adjacent fields, measured along the waveguide axis direction, can be determined.

After the x-ray mask has been developed and electroplated, the outrigger structures are imaged at high magnification with the electron-beam system. The relative offset in position between the two gratings of each outrigger structure can then be measured by comparing their spatial phase. The outrigger gratings are designed so that the offset between the gratings is equal in magnitude to the interfield stitching error.⁴

The stitching error data corresponding to the mask used to fabricate the single-pole resonator devices are shown in Fig. 3(a). The corresponding mean and standard deviation are 32 and 13 nm, respectively. These errors are significantly larger than the apparent misalignment data obtained from phase-locking alignment during the e-beam exposure of the gratings, where the mean was 0.9 nm and standard deviation was 0.3 nm, see Fig. 3(b). We are uncertain as to the origin of this large differential, but suspect an independent source of error, possibly related to the fact that we perform precise alignment (i.e., phase locking) in only one dimension, along the

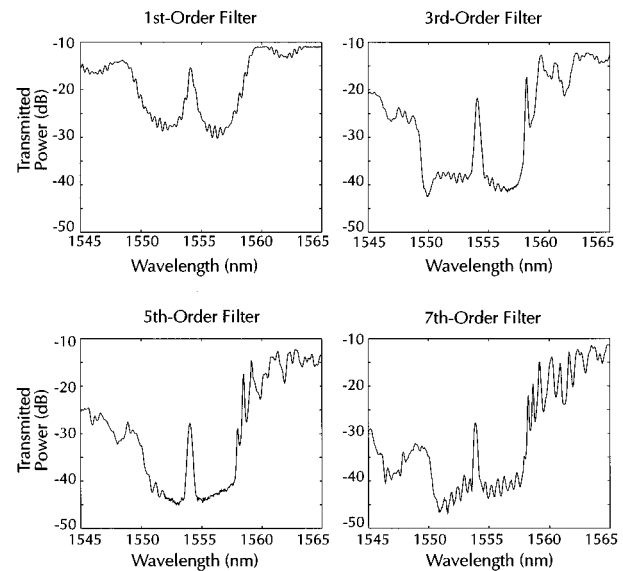


Fig. 5. The optical transmission response of first-, third-, fifth-, and seventh-order Gaussian multiple-pole filters. While the 0.1 nm resolution limit of the optical spectrum analyzer does not well resolve the center filter response, the side lobes on the long-wavelength of the stopband are indicative of a Gaussian multiple-pole filter response.

reference-grating k -vector axis, while alignment in the perpendicular direction is uncorrected. In fact, we utilized a coordinate system in which the y beam deflection was parallel to the fiducial grating lines, while the x beam deflection was parallel to the waveguide axis.⁸ Consequently, the two deflection axes deviated from orthogonality by the degree to which the waveguide axis was originally misaligned to the k vector of the fiducial grating axis, or a 0.05° error in this case.

The systematic component of the stitching error results largely in a shift of the entire filter spectrum whereas the stochastic component distorts the spread of the pole locations. However, general analysis of the pole location error as a function of stitching errors is not possible because the connection between a quarter-wave-shifted distributed Bragg resonator and the mathematical description of a resonator is broken by the introduction of stitching errors. Only the transmission or reflection spectrum as a whole can be analyzed with stitching errors present. The latter analysis has been done for a single-pole resonator⁹ with the general result that the gratings should be coherent to better than $\lambda/120$, where λ is the optical wavelength in the waveguide. While we have achieved no better than $\lambda/70$, we believe that once the sources of error have been identified and corrected, the fidelity of the e-beam written gratings will more closely approach that of a reference generated by interferometric lithography.

IV. OPTICAL TRANSMISSION RESULTS

Optical transmission measurements of twelve single-pole resonators and several higher-order Gaussian filters were performed by coupling the amplified spontaneous emission of an erbium-doped fiber amplifier onto the waveguide chip through a micromachined fiber lens.¹⁰ The transmitted light

was coupled out with a 40 \times microscope objective and directed to an optical spectrum analyzer that has a 0.1 nm resolution.

Figure 4(a) shows the transmission response of a single-pole filter that spanned nine e-beam fields. The single-pole resonance at the center of the stopband has a FWHM of approximately 1.5 Å. The high-frequency fringes in the transmission response are the result of Fabry-Pérot reflections between either facet and the grating. Figure 4(b) plots the deviation from stopband center of resonances from 12 resonators of different grating periods and grating lengths. All of the 12 resonances lie within a ± 1 Å error band, or $\pm 3\%$ of the stopband width.

Figure 5 shows the transmission response of four multiple-pole Gaussian filters. Due to problems with fabrication, the optical loss on this chip was higher than the single-pole filter chip, thereby causing the peak resonance intensity to fall quickly with filter order. Nonetheless, there is a clear filter sharpening between the first- and third- and fifth- and seventh-order filter. The 0.1 nm resolution of the optical spectrum analyzer limits the degree to which we can measure the filter roll off as the filter order is increased. However, the sidebands on the long-wavelength side of the stopband correspond well with the side bands anticipated as a result of the multiple quarter-wave shifts.

ACKNOWLEDGMENTS

The authors wish to acknowledge S. Rishton of the IBM T. J. Watson Research Center for his support and use of the IBM VS-6 electron-beam lithography system. This work was supported by the Semiconductor Research Corporation (SRC), the National Science Foundation (NSF), the Army Research Office (ARO), the Advanced Research Projects Agency (ARPA), the National Center for Integrated Photonic Technologies (Contract No. 542383), and the Advanced Concepts Committee of MIT Lincoln Laboratory (Contract No. BX5411).

¹H. A. Haus and C. V. Shank, *J. Quantum Electron.* **12**, 532 (1976).

²H. A. Haus and R. V. Schmidt, *Electron. Lett.* **13**, 445 (1977).

³H. A. Haus, and Y. Lai, *J. Quantum Electron.* **28**, 205 (1992).

⁴J. Ferrera, V. V. Wong, S. Rishton, V. Boegli, E. H. Anderson, D. P. Kern, and H. I. Smith, *J. Vac. Sci. Technol. B* **11**, 2342 (1993).

⁵V. V. Wong, J. Ferrera, J. N. Damask, J. Carter, E. E. Moon, H. A. Haus, H. I. Smith, and S. Rishton, *J. Vac. Sci. Technol. B* **12**, 3744 (1994).

⁶H. Y.-F. Lam, *Analog and Digital Filters: Design and Realization* (Prentice-Hall, Englewood Cliffs, NJ, 1979).

⁷Courtesy of Don Hofer, IBM Almaden Research Center, San Jose, CA.

⁸See Ref. 5 for figure of fiducial gratings, device gratings, and alignment axes.

⁹J. N. Damask, J. Ferrera, V. V. Wong, H. I. Smith, and H. A. Haus, *Proc. SPIE* **2213**, 137 (1994).

¹⁰The authors wish to thank Photonic Packaging Technologies, Inc., Oregon, for providing the micromachined fiber lenses.